ARTICLES

Calculation of anomalous phonons and the hcp-bcc phase transition in zirconium

U. Pinsook and G. J. Ackland
Department of Physics and Astronomy, The University of Edinburgh, Edinburgh, EH9 3JZ, Scotland, United Kingdom
(Received 13 January 1999)

Using molecular dynamics with a many-body potential fitted to properties of zirconium we study the behavior of phonons at high temperature in the bcc lattice; in particular, the T_{1N} mode which according to the Nishiyama-Wassermann mechanism is the cause of the martensitic transition to hcp in group-IV transition metals. This phonon frequency softens towards the transition but does not tend to zero frequency. In contrast to the fast kinetics of the bcc→hcp transition, the reverse process, i.e., hcp→bcc, is not observed in standard molecular dynamics: it can be induced if the T_{1N} phonon is perturbatively excited in the martensitic phase. The sluggishness of the reverse process is attributed to the fact that in the low-temperature hcp phase, the equivalent oscillation to T_{1N} involves two modes with different frequency. The bcc to hcp transition is a first-order transition and occurs in such a way that most of the reversed bcc atoms obey Nishiyama-Wassermann rules, i.e., the path of transformation is reversible. However, there is some plastic damage which is not recovered. [S0163-1829(99)10021-3]

I. INTRODUCTION

A martensitic transition is a structural phase transition which involves little movement of atoms during transformation. In group-IV transition metals, i.e., titanium, zirconium, and hafnium, a transition from body-centered-cubic to hexagonal-close-packed structure is observed on lowering the temperature. The atomistic mechanism for this transition has been described by the Nishiyama-Wassermann (NW) rules.[1–3] Zirconium is the best representative of the group for simulation purposes: unlike titanium, zirconium has no magnetic moment and the phase transition is purely mechanical.[4] The experimentally determined transition temperature T_0 is 1136 K.

The nature of the kinetics of this type of transition has been widely investigated. In 1947 Zener[5] studied β brass and proposed a soft-mode model for the stability of the bcc structure in which the shear modulus $\frac{1}{2}(C_{11}-C_{12})$ becomes lowered and approaches zero at the transition temperature. Below the transition temperature each unit cell in the lattice becomes mechanically unstable and a phase transition occurs. A similar model by Friedel concentrates on a particular short-wavelength phonon becoming unstable.[6] However, the mechanism is not always so simple: in general the phonon mode will have lower symmetry than the crystal and hence will couple to the macroscopic strain. In this case one of the single-crystal elastic constants will tend to zero at the transition, but there is no pure phonon instability. The phase transition occurs by a distortion involving both the phonon and the strain, which is in general accommodated by the formation of a microstructure.

The latter is the case in zirconium. According to the mechanism proposed by Nishiyama and Wassermann (NW), significant finite strain is required in addition to the T_{1N} phonon.

Using inelastic neutron scattering, the phonon dispersion curve of zirconium has been measured[7,8] and revised.[9,10] This shows that the T_{1N} phonon is softened a little toward the transition temperature with a slope of 0.0008 THz/K. Although the softening is consistent with the soft-mode model in which T_{1N} is the cause of the transition, this phonon has a finite frequency of about 1.08 THz at the transition temperature[9] implying a coupling with the strain. The neutron-measured phonon does not incorporate coupling to an infinite wavelength strain, this coupling explains the occurence of the transition prior to the T_{1N}-mode frequency going to zero.

Several theoretical models have been proposed in order to describe the experimental results. May, Müller, and Strauch[11] studied the vibrational properties of zirconium by using a Born-Mayer-type potential. They concluded that zirconium manifests line broadening, line shift, and interference which are the main features of a strong anharmonic system. *Ab initio* work by Ye *et al.*[12] employed the frozen phonon method and discovered that the modes along the salient phonon branch, i.e., Γ-N $\mathbf{k}=[\xi\xi 0]$, are strongly coupled. Willaime and Massobrio[13,14] derived a four-parameter embedded atom method (EAM) potential for zirconium: In harmonic and quasiharmonic regimes, the T_{1N} phonon becomes unstable, but using molecular dynamics they found that the phonon is dynamically stable and has a finite frequency at higher temperature. From the fact that the anharmonic effect is fully included via the interatomic potential, this result confirms that the anharmonic effect has an important role for stabilizing the bcc lattice.

From the thermodynamic point of view, theoretical approaches such as Landau-type theory, mean-field theory,[15] and self-consistent phonon theory[16,17] led to the same conclusion that the excess vibrational entropy stabilizes the high-temperature phase. This can be explained as follows: First, the T_{1N} phonon has a peculiar low frequency and thus

can be excited easily.[16,17] Consequently, the vibrational entropy of the system becomes large enough to stabilize the bcc structure. Second, at the transition temperature, the frequency of the phonon is still finite but magnitude of the fluctuation is decreasing and therefore its vibrational entropy is no longer sufficient to stabilize the bcc structure and the transition to hcp structure takes place. This is in a good agreement with the experimental results. The phonon density of states in a low-frequency region around 1.69 THz is lowered with decreasing temperature.[9] The argument of excess entropy stabilizing the high-temperature phase is also applied to the similar martensitic transition in NiAl alloys,[18] however, since the transition in zirconium occurs above the Debye temperature the phonon entropy argument should be treated with caution.

Based on these observations, Lindgård and Mouritsen[2,19] used strain components as order parameters in a Landau theory to study martensitic transition in zirconium. A similar method is applied by Gooding and Krumhansl[20] to study the bcc$\rightarrow 9R$ transition in Li. They used a corresponding phonon as an order parameter and combined the phonon with strain components. Both works show that the transition is first order and stacking faults can be formed as a metastable state.

Ab initio calculations have shown that the density of states at the Fermi energy in bcc is higher than in hcp.[4,21,22] It is therefore possible that the phase transition is due to excess electronic entropy. However, as we show here, and as is known from the electronic structure calculations, the effect of this high density of states is to destabilize the ideal bcc structure (i.e., all atoms on their lattice positions) used to calculate the density of states. Thus the density of states derived from this ideal structure may no longer be a good model for the high-pressure structure.

Despite this clear picture of how and why the bcc structure transforms into the hcp, there is no further study of the T_{1N} phonon mode in the low-temperature phase. It is suggested that the phonon mode might split into several modes in the hcp[23] and become much stiffer.[16,17] However, there is no systematic proof of this relation. Moreover, the role of T_{1N}-equivalent mode in hcp to the reverse transition remains unsolved.

In the present work, we use molecular dynamics to calculate the phonon properties of the bcc structure in zirconium using a many-body potential which is known to reproduce the phase transition via the NW mechanism.

Simulations in which the temperature is lowered through T_c are performed in order to allow the phase transition. The evolution of T_{1N} phonon is monitored. We attempt to raise the temperature to investigate the reverse transition, but in the limit of our finite-size molecular dynamics, the reversed process is not observed. Nevertheless, we can induce the hcp to bcc transition by exciting the T_{1N} equivalent mode in the martensitic microstructure.

Throughout this paper we use the term martensite microstructure to mean the twinned hcp microstructure which has been produced from the bcc phase via the phase transition. It is not a pure single crystal, but contains several hcp variants, twin boundaries, and some stacking faults[3] which one might expect to act as nucleation centers for the reverse transition. In Ref. 3 it was shown that the transformation path is not perfectly microscopically reversible in the sense that a minority of the atoms in the hcp structure have different neighbors than would be predicted from the NW mechanism, having moved relative distances of order of the lattice parameter. Although this microscopic irreversibility is at variance with the Nishiyama-Wassermann mechanism, the majority of the atoms were found to have the expected neighbors.

II. MOLECULAR DYNAMICS

In our simulations we use a Finnis-Sinclair-type potential[24] which has the form

$$E_i=\frac{1}{2}\sum_j V(r_{ij})-\sqrt{\sum_j \phi(r_{ij})}, \tag{1}$$

where $V(r_{ij})$ represents the pair repulsive energy, ϕ_i is a parameterized pairwise interaction representing the square of the tight-binding hopping integral, and its square root represents the cohesive energy of a partialy filled band in the assumption of local charge neutrality.[25] The cubic spline functional form is chosen for $V(r_{ij})$ and ϕ_i.[26] The potential was fitted to properties of the hcp structure only, namely the anisotropic elastic properties of zirconium, the 1.595 nonideal c/a ratio, the lattice parameter, vacancy formation, and cohesive energy of the hcp structure.[27] Although fitted only to the hcp phase, the potential is known to reproduce a good description of both bcc and hcp phases: in particular, the transition temperature observed by classical molecular dynamics at large system size lies between 1330 and 1390 K,[3] depending slightly on choice of boundary conditions and thermostats. Further details of the potential are discussed elsewhere.[27]

We solve Newton's equations of motion by using a molecular-dynamics code.[28,29] The integration scheme is a fourth-order Gear predictor-corrector algorithm. The time step is equal to 1 fs. Temperature is regulated by a Nose-Hoover[30–32] thermostat. The initial configuration is a homogeneous bcc lattice with the equilibrium value of the lattice parameter corresponding to the thermal expansion predicted by the potential at each temperature, as found by a preliminary series of constant pressure simulations. This variation of bcc lattice parameter with temperature is shown in Fig. 1. In all calculations, the unit cell is oriented along $(100)_{bcc}$, $(010)_{bcc}$, and $(001)_{bcc}$, unless otherwise stated.

III. NORMAL-MODE CALCULATION IN THE BCC PHASE

In order to study a particular vibrational mode in a crystal, we first define the eigenvector of that mode. To do this the displacements of atoms in solid are written in terms of a complete set of independent coordinates[33] as

$$\alpha_{\mathbf{k}}(t)=\sum_i [\mathbf{r}_i(t)-\mathbf{l}_i]\cdot\mathbf{e}_{\mathbf{k}}\cos(\mathbf{k}\cdot\mathbf{l}_i), \tag{2}$$

where $\mathbf{k}$ is a wave vector, $\mathbf{e}_{\mathbf{k}}$ is a corresponding eigenvector of the mode $\mathbf{k}$, $\mathbf{l}_i$ is a lattice vector, and $\mathbf{r}_i$ is the position of atom i. These coordinates are chosen to be the normal modes of the bcc crystal, with $\mathbf{e}_{\mathbf{k}}$ determined from a lattice-dynamics calculation at 0 K. Consequently, their vibrations are classical objects analogous to phonons (which are quan-

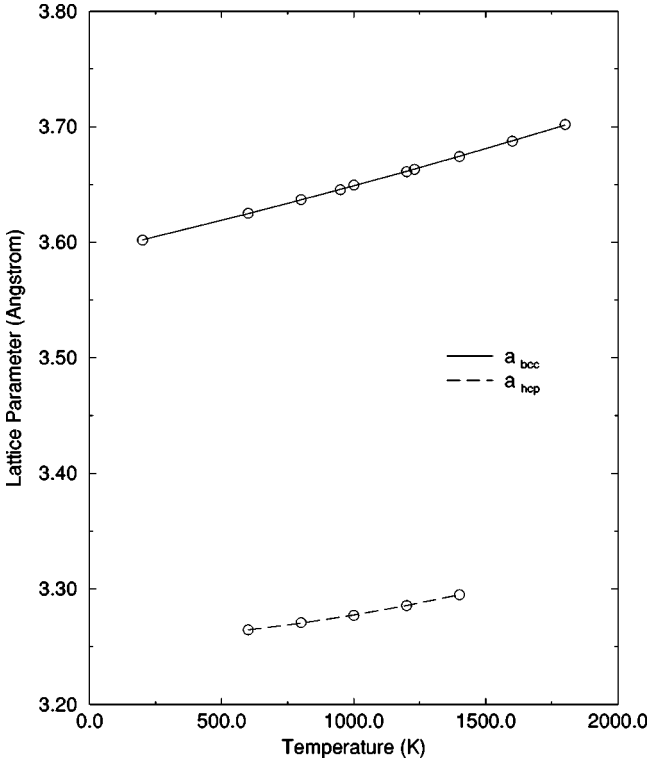

FIG. 1. Variation of the equilibrium bcc lattice parameter against temperature. Each point was calculated from a constant pressure molecular-dynamics calculation. Below the transition pressure the data is collected for a supercooled bcc phase which remains stable for a few ps.

tized) and with the same frequency, and can be compared directly to neutron-scattering data.

If the crystal were perfectly harmonic, the evolution of the normal coordinates could be written as

$$\alpha_{\mathbf{k}}(t) = A\cos(\omega_{\mathbf{k}} t + \varphi_{\mathbf{k}}), \tag{3}$$

where A is an amplitude, $\omega_{\mathbf{k}}$ is the frequency of the mode, and $\varphi_{\mathbf{k}}$ is a phase factor.

We define the autocorrelation function for this mode as $\langle \alpha_{\mathbf{k}}(t)\alpha_{\mathbf{k}}(0)\rangle$. In the harmonic case its Fourier transform is then simply a delta function at $\omega_{\mathbf{k}}$.

At high temperatures, anharmonic effects cause the evolution of the modes to depend on the excitation of other modes. Now the Fourier transform of the autocorrelation function will exhibit a peak at $\omega_{\mathbf{k}}$, broadened by these coupling effects. Moreover, if the mode itself is anharmonic, further broadening will occur and the peak position will be dependent on temperature.

Finally, if $e_{\mathbf{k}}$ is not a normal mode, the Fourier transform will consist of peaks at each of the normal modes of which $e_{\mathbf{k}}$ is comprised. For example, if we take $e_{\mathbf{k}}=1$, there will be a peak for each phonon with wave vector $\mathbf{k}$.

In the simulation box, there are only a certain number of wave vectors that are allowed due to the finite number of atoms. The possible wave vectors are given by integers n_k, n_l, and n_m such that

$$\mathbf{k} = \left(\frac{2\pi n_k}{a}, \frac{2\pi n_k}{b}, \frac{2\pi n_k}{c}\right), \tag{4}$$

TABLE I. $\mathbf{k}_1=[\xi\xi 2\xi]$.

ξ	T_1	T_2	L
0.0625	0.52	0.86	1.86
0.1250	1.06	1.75	3.50
0.1875	1.56	2.84	4.57
0.2500	1.57	3.86	5.17
0.3125	1.91	4.49	4.79
0.3750	1.79	5.09	4.21
0.4375	1.20	5.40	3.60
0.5000	0.53	5.51	3.33

where a, b, and c are the lengths of the axes of the orthorhombic simulation cell. The maximum allowed value of n_k, n_l, and n_m is determined by the number of bcc primitive unit cells along each axis.

Thus once the vibrations of the structure are projected onto these normal modes, it is straightforward to extract the frequency of a specific phonon at a particular temperature by Fourier transforming the ensemble-averaged position $\langle \alpha_{\mathbf{k}}(0)\cdot\alpha_{\mathbf{k}}(t)\rangle$ or velocity $\langle \dot{\alpha}_{\mathbf{k}}(0)\cdot\dot{\alpha}_{\mathbf{k}}(t)\rangle$ autocorrelation function. We will use this method to determine the finite-T phonon dispersion relation from our molecular-dynamics (MD) simulation.

A difficulty arises when a harmonic mode basis is applied to study a strongly anharmonic system because vibrations of the normal-mode coordinates are no longer independent: in quantum language the phonons are scattered. However, in the present case we found it was always possible to unambiguously identify the peaks in the Fourier transform.

An alternative approach led Dickey and Paskin[33] to introduce a perturbative normal-mode calculation in which a phonon is artificially excited at a particular time. The perturbation is defined as

$$\mathbf{r}_i'(t) = \mathbf{r}_i(t) + \epsilon\cos(\mathbf{k}\cdot\mathbf{l}_i)\mathbf{e}_{\mathbf{k}}, \tag{5}$$

where $\mathbf{r}'$ and $\mathbf{r}$ are perturbed and unperturbed atomic position, respectively. The advantages of this method are that both the phonon frequency and its lifetime can be calculated within a short simulation period. This is because the additional energy of the perturbed mode is dispersed into other modes soon after the perturbation. However, when Willaime and Massobrio[13,14] used this method to study T_{1N} phonon in the bcc structure they found that the frequency of the phonon is dependent on the strength of the perturbation ϵ, showing that the phonon itself is strongly anharmonic.

Since our calculations are designed to study very anharmonic phonons, we avoid all these difficulties and ensure the statistical reliability by calculating phonon frequencies direct from the time evolution of normal-mode coordinates from a long simulation, i.e., 40 ps and averaging over six samples. We will adopt the perturbative approach later when considering the reverse transition from hcp to bcc.

Thus we construct the finite temperature phonon dispersion curve. We simulate 8192 bcc atoms at 1400 K and present the phonon-dispersion relation along four branches which are $\mathbf{k}_1=[\xi\xi 2\xi]$, $\mathbf{k}_2=[\xi\xi 0]$, $\mathbf{k}_3=[00\xi]$, and $\mathbf{k}_4=[\xi\xi\xi]$. The results are shown in Tables I–IV and compared with the experimental[9] data for zirconium in Fig. 2.

TABLE II. $\mathbf{k}_2=[\xi\xi 0]$.

ξ	T_1	T_2	L
0.0625	0.08	1.06	0.58
0.1250	0.16	2.10	1.16
0.1875	0.32	3.14	1.69
0.2500	0.40	3.92	2.18
0.3125	0.49	4.66	2.71
0.3750	0.59	5.12	3.02
0.4375	0.56	5.38	3.19
0.5000	0.53	5.51	3.33

The results are generally in good agreement with the experiment: since the potential was not fitted to any properties of this bcc structure this gives us confidence to proceed. The only discrepancy is in the value of the Γ-N branch phonons which are somewhat lower than experiment. This is consistent with the fact that the phase-transition temperature for the potential is higher than for real zirconium.

It is also possible to obtain phonon-dispersion relations by lattice dynamics.[34] Force constants and dynamical matrix elements can be obtained analytically from doubly differentiating the potential which introduces slight complications due to its many-body nature.[35] Unlike experiment and MD, which measure correlation functions, lattice dynamics directly measures the harmonic term in the potential-energy surface: no anharmonic effects are incorporated, although in the quasiharmonic approach the lattice dynamics is performed at different lattice parameters according to the temperature.

Lattice dynamics results for the current potential at a bcc lattice parameter of 3.67 Å (corresponding to 1400 K) are plotted in Fig. 1. Again, good agreement with both experiment and MD can be seen with the dramatic exception of the T_{1N} branch, where the harmonic phonon frequency is imaginary—i.e., the expanded bcc lattice is unstable with respect to this distortion.

The failure of the lattice dynamics calculation to reproduce the experimentally observed behavior provides dramatic evidence for the importance of anharmonicity in the system. Moreover, it explains why the visualization method used in Ref. 3—quenching the structure to 0 K and examining the neighbors of each atom—never gives any bcc-coordinated atoms.

A further failing of the quasiharmonic approach is that it predicts that the T_{1N} phonon becomes stiffer with reduced volume (i.e., reduced temperature). Indeed, it is actually stable at the zero-temperature equilibrium volume for (metastable) bcc zirconium. This suggests that the high-pressure bcc phase in the zirconium phase diagram has a quite different character from the dynamically stabilized high-T bcc phase.

TABLE III. $\mathbf{k}_3=[00\xi]$.

ξ	T	L
0.1250	0.85	1.25
0.2500	1.69	2.46
0.3750	2.64	3.39
0.5000	3.43	4.13
0.6250	4.13	4.53
0.7500	4.49	4.65
0.8750	4.72	4.84
1.0000	4.76	4.76

TABLE IV. $\mathbf{k}_4=[\xi\xi\xi]$.

ξ	T	L
0.1250	0.86	2.63
0.2500	1.97	4.43
0.3750	3.23	5.00
0.5000	4.26	4.26
0.6250	4.38	2.18
0.6666	4.60	1.79
0.7500	4.80	2.34
0.8750	5.03	4.07
1.0000	4.76	4.76

The frequency of T_{1N} phonon is calculated by MD in constant volume and constant temperature mode at 1400, 1600, and 1800 K as shown in Fig. 3. The slope is 0.0003 THz/K.

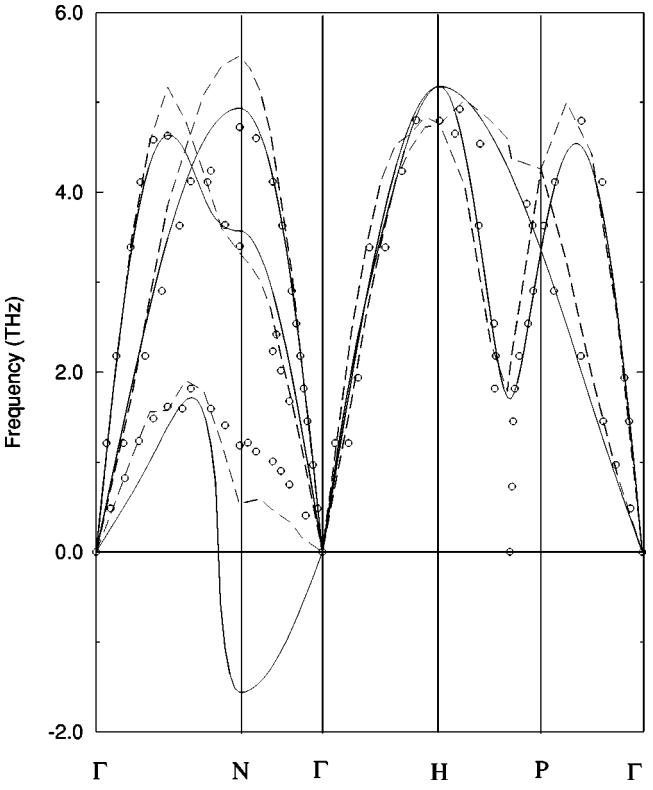

FIG. 2. Phonon dispersion curve at $T=1400$ K. Dashed lines are the results of the MD calculation as described in the text. Circles are experimental results taken from Ref. 9. Solid lines represent quasiharmonic lattice-dynamics calculations for perfect bcc at the volume implied by the MD thermal expansion in Fig. 1. Imaginary frequencies corresponding to unstable phonons are shown as negative.

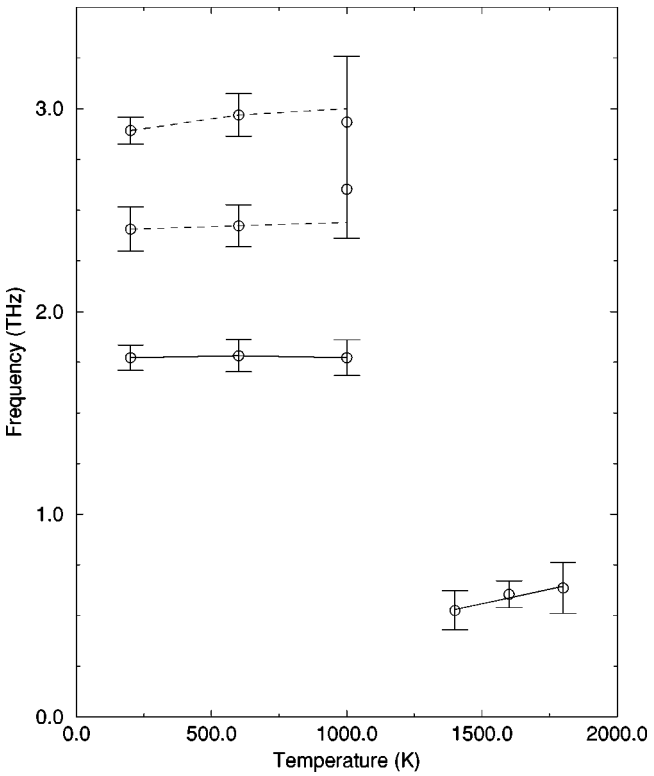

FIG. 3. Temperature dependence of T_{1N} phonon in the bcc phase at $T>1390$ K and the peaks of the Fourier transform for the equivalent mode in the hcp phase at $T<1390$ K. Each point is taken from an average over several MD runs, and the error bars reflect the spread of the results. At 1000 K for some microstructures it proved impossible to distinguish between the two highest frequency peaks.

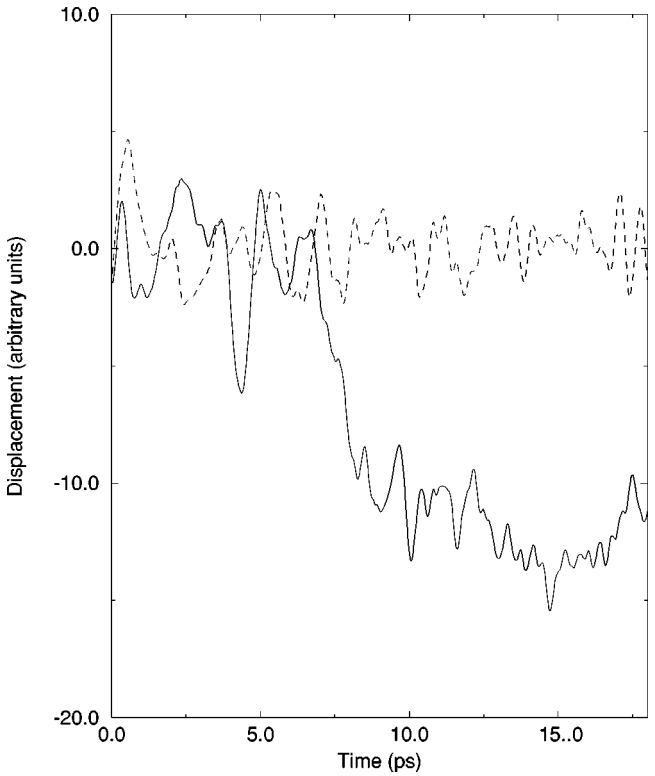

FIG. 4. Time evolution of the α_N coordinate following rapid cooling from 1400–1000 K, showing large fluctuations in the unstable bcc phase, followed by a discrete shift of the mean at the phase transition and subsequent stable oscillations in the hcp phase.

IV. THE "T_{1N} MODE" IN THE HCP STRUCTURE

When the system undergoes a phase transition to the low-temperature hcp structure, there are six possible martensitic variants which could occur, each corresponding to an NW transition involving a particular T_{1N} mode.[36] In practice, a subset of three of these are selected, depending on the specific martensite growth plane, and a strain compensating microstructure involving these three hcp variants is formed.[3]

While taking the material through its phase transition, we have continued to evaluate the time evolution the coordinate $\alpha_{\mathbf{N}}(t)$, which corresponds to the T_{1N} mode. According to the NW mechanism, within a single variant, one of the sets of $[011]_{bcc}$ planes becomes the basal planes in hcp, four become pyramidal planes, and one becomes prism planes.

Figure 4 shows typical plots of the $\alpha_{\mathbf{N}}(t)$ associated with the operative NW mechanism through the phase transition. In the bcc phase, the fluctuation of those planes is (by construction) around zero displacement $\int \alpha_{\mathbf{N}}(t)dt=0$. After the transition, the fluctuation is displaced away from zero point indicating the structural change. This shows that in spite of the appearance of microstructure $\langle \alpha_{\mathbf{N}}(t)\rangle$ is a good order parameter for the transition.

When the system reached an equilibrium in the martensite phase, the T_{1N} "phonon" is projected out at 200, 600, and 1000 K. To investigate the T_{1N}-equivalent mode in the hcp phase we continue to follow the fluctuation and displacement of the coordinate α_N. After the transition we took a Fourier transform of the $\alpha_{\mathbf{N}}(t)$ autocorrelation function in the hcp phase. The data is rather noisy, so we have applied a maximum entropy procedure across various runs which enables us to distinguish the peaks corresponding to the hcp phonons which make up $\alpha_{\mathbf{N}}(t)$.

The discrete Fourier transforms of the time evolution of $\langle \alpha_N(t)\rangle$ in the hcp phase are shown Figs. 5 and 6, together with the maximum entropy smoothing and the actual data in the insets.

For three of the modes (typified by Fig. 5) we find that the time averaged $\langle \alpha_{\mathbf{N}}(t)\rangle$ changes from zero to a finite value at the transition. This value is related to the amount of each variant in the resulting microstructure, but not in a straightforward way because both positive and negative $\alpha_{\mathbf{N}}(t)$ give rise to equivalent hcp variants. For the $\alpha_{\mathbf{N}}$ involved in the transition there is a large peak centered on zero corresponding to the slow evolution of the microstructure and the coupling of the mode to the strain. There are also two distinct peaks at relatively low frequency, showing that the coordinate $\alpha_{\mathbf{N}}$ no longer represents a normal mode.

A typical example of one of the three T_{1N} modes which are related to variants which do not appear in the microstructure is shown in Fig. 6. This has has a time-averaged value of $\int \alpha_{\mathbf{k}}(t)dt=0$ and shows two peaks in the smoothed Fourier transform. This indicates that there is no normal mode in the hcp which is equivalent to the mode in bcc which is responsible for the transition.

Figure 3 shows frequencies of these modes evaluated at different temperatures. Unlike the T_{1N} mode in bcc no clear temperature dependence can readily be determined.

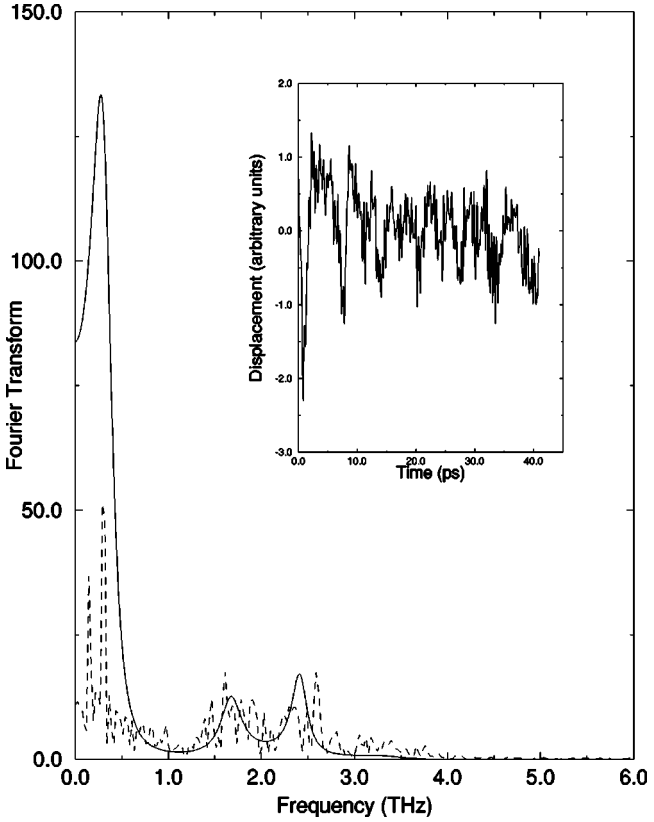

FIG. 5. Typical time evolution of the α_N coordinate for a T_{1N} mode in the hcp phase which is involved in the transition via the NW mechanism following rapid cooling from 1400–1000 K. The main figure shows the discrete Fourier transform of the data (dotted line) and the result of a maximum entropy smoothing of this data (solid line), while the inset shows the data $\alpha_N(t)$ itself from which a constant is subtracted to make the mean value zero prior to taking the Fourier transform.

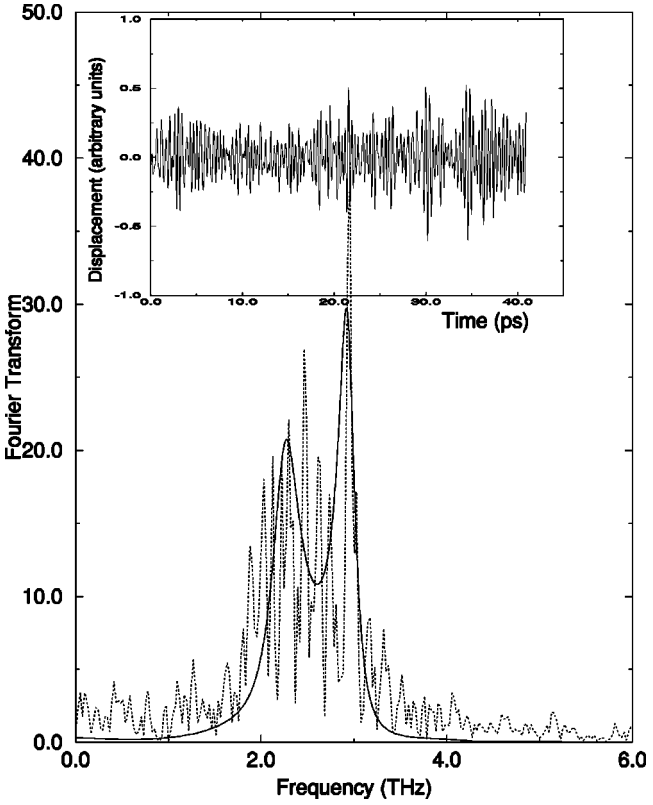

FIG. 6. Typical time evolution of the α_N coordinate for a T_{1N} mode which is not involved in the transition following rapid cooling from 1400–1000 K. The main figure shows the discrete Fourier transform of the data (dotted line) and the result of a maximum entropy smoothing of this data (solid line), while the inset shows the data $\alpha_N(t)$ itself.

V. THE REVERSE PHASE TRANSITION, HCP-BCC

To investigate the hcp-bcc transition we carried out a series of simulations comprising up to 75 000 atoms, initially in the pure hcp structure or the martensitic hcp microstructure. Simulations lasted 50 ps and involved heating to temperatures between the transition temperature and the point at which the crystal melts. Twenty calculations were performed at varying final temperatures and starting conditions. The hcp to bcc transition has not been observed at any temperature, no matter how hcp structure is defined, i.e., pure hcp or martensite microstructure.

The possible explanation is that the T_{1N} phonon splits into two or three normal modes in the hcp phase with different frequencies. Furthermore, it becomes stiffer as discussed in the last section. Thus to obtain the bcc phase via the reverse Nishiyama-Wassermann mechanism, the transition dynamics require simultaneous coherent fluctuation from several normal modes, rather than one. Since the normal modes have different frequencies, the required vibrations cannot remain in phase and the phonon-driven transition mechanism cannot function. In fact, even if the normal modes had the same frequency, the fact that the excited eigenvector, a linear combination of the degenerate eigenvectors, may not be exactly the right combination to cause the transition.

The above reasoning does suggest that if we can artificially stimulate the vibration corresponding to the T_{1N} phonon, and if the stimulation is strong enough, it might be possible to induce the hcp to bcc transition. To prove this, we impose the perturbation scheme defined by Eq. (5) to excite the T_{1N} phonon in the martensitic phase and perform the simulation at 1400 K where the bcc phase is stable. We use the martensitic hcp phase because we know exactly which $\mathbf{e_N}$ eigenvector corresponds to the T_{1N} phonon which was involved in the transition. We found that the strength of perturbation ϵ required to induce the hcp to bcc transition is 5.7% of the lattice parameter.

The eigenvector $\mathbf{e_N}$ is common to the entire Γ-N branch and so we tried exciting a phonon at $\mathbf{k}=0.56\mathbf{k_N}$ to see if it could induce the transition. Again this was successful, although the size of perturbation required was much larger, 28.3% of the lattice parameter.[37]

It is interesting that this is sufficient to induce the hcp to bcc process, because in the previous work,[13,14] perturbation strengths of up to 8.5% of the lattice parameter were used to study the T_{1N} phonon frequency.

The question of whether the high-temperature structure is bcc or hcp structures can be addressed in a number of ways. One is to consider thermodynamic properties of the whole system, the difference in cohesive energy is 0.03 eV/atom, the difference in volume is 0.6 Å^3/atom. In constant volume simulation, the stress tensor will change. In constant stress, the box components will change. All these features are in-

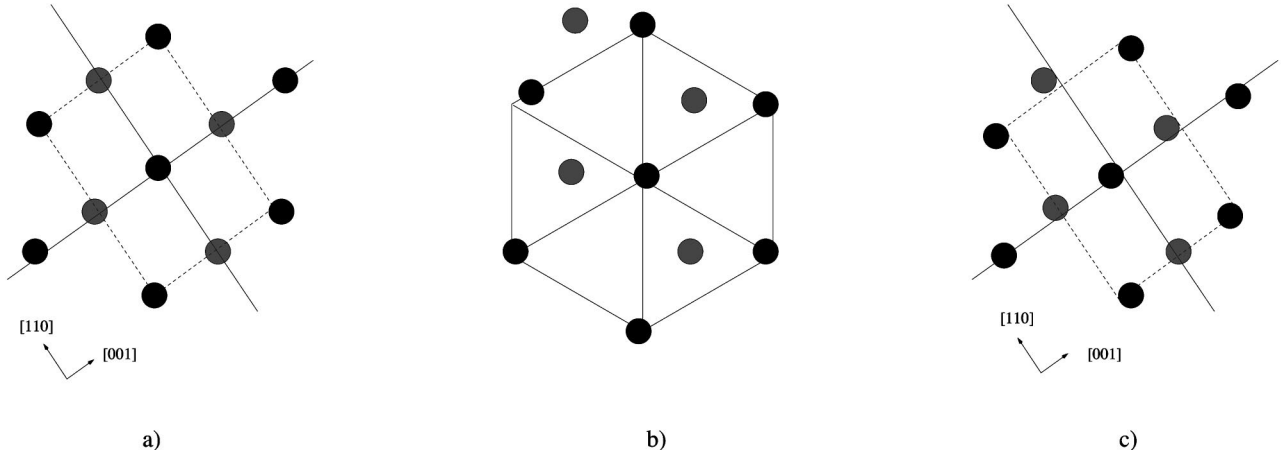

FIG. 7. Atomic pictures taken from a typical simulation of the bcc to hcp and the hcp to bcc transition. (a) Initial bcc structure; (b) microstructure after the martensitic transition; (c) induced bcc phase. Notice that it has some thermal fluctuation. Black and grey circles label different layers.

dicative of the phase under observation, and their discontinuous change suggests the phase transition, but the most important tools are the radial distribution function, the nearest-neighbor angular distribution function, and the assignment of a local crystal structure to each atom by fitting a template to a snapshot of its local environment.[3] Figure 7 shows typical local ordering of a few atoms through the complete bcc $\rightarrow$martensite$\rightarrow$bcc phase transition cycle. In Fig. 8 this cycle is further studied by quenching configurations to zero kelvin and measuring the ''local crystal structure'' of each atom. Figure 8(a) shows the perfect bcc lattice used as a starting condition. Figure 8(b) shows the characteristic strain-compensating hcp microstructure, while Fig. 8(c) shows that the induced bcc phase contains predominantly bcc atoms but that significant numbers now have locally hcp-type order.

VI. CONCLUSIONS

We have used molecular-dynamics simulation to study the properties of the phonons in the high-temperature bcc-phase of zirconium. The high-temperature phonon dispersion relation in the bcc lattice is established and it is in a good agreement with the experimental results. The frequency of the T_{1N} phonon is 0.53 THz at 1400 K with a temperature dependence of 0.0003 THz/K. Quasiharmonic lattice dynamics is shown to be inadequate to describe this phonon, predicting it to be unstable at the volume of the simulation. Lattice dynamics does show that the phonon becomes stable as the volume is reduced. This indicates that while the high-temperature bcc phase is dynamically stabilized by anharmonic effects against the T_{1N} mechanical instability, the high-pressure bcc phase is likely to be a conventional harmonic crystal. It would be interesting to investigate zirconium at simultaneous high temperature and pressure to see whether an isostructural transition exists between these two phases.

Although the phonon softens toward the transition, its frequency does not go to zero. Thus the transition is first order and must be nucleated by a large fluctuation in the phonon amplitude, together with a coupling to the strain. Of course,

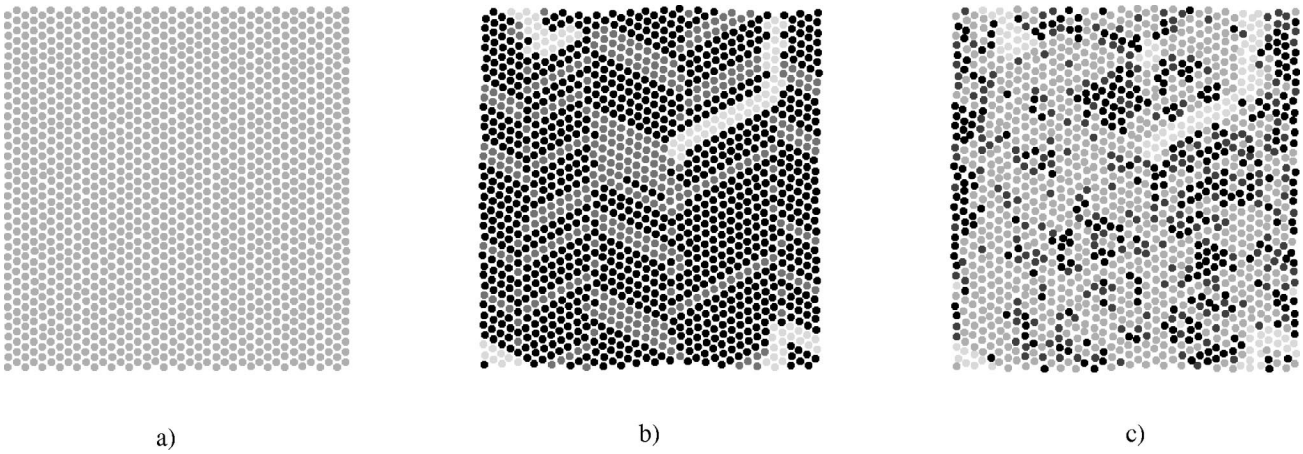

FIG. 8. Snapshots of a slice through the simulation cell showing the transformation from bcc to hcp by cooling, and the reverse transition by heating and excitation of the approprite vibrational mode. The coloring of the atoms is determined by fitting a template of the nearest-neighbor shell expected for bcc, fcc, or hcp to each atom. The atoms are then shaded as follows: black atoms have local hcp coordination with neighbors as expected from the NW transition mechanism; dark grey atoms have local fcc coordination; mid grey atoms have bcc coordination while light grey atoms have a different set of neighbors from their original 14, indicating irreversible plastic deformation. (a) Initial bcc; (b) martensitic hcp; (c) induced bcc.

it is the compensation for this strain which gives rise to the martensitic microstructure.

We have continued to study the fluctuation of atomic planes that used to be the T_{1N} phonon after the phase transition to a martensitic hcp occurs at around 1350 K. It is no longer a pure phonon mode. This means that the reverse Nishiyama-Wassermann mechanism cannot operate by phonon fluctuations since it would require two phonons to be excited simultaneously and coherently. Statistically, this is a far less likely scenario than the single mode excitation required for transition from bcc, and consequently we observe that the reverse transition can only occur (on the time scale of our simulations) if such a simultaneous, phonon excitation is induced artificially. We believe that this may be a rather general result in a wide class of martensitic transitions, and may explain, for example, the different mechanisms observed for the forward and back transitions in iron where it has been reported that the fcc-bcc transition occurs via the Bain deformation while the reverse bcc-fcc transition follows the Burgers path.[38]

ACKNOWLEDGMENTS

This work was supported by the EPSRC and the Royal Thai government through the IPST.

[1] Z. Nishiyama, *Martensitic Transformations* (Academic Press, New York, 1978).
[2] P.-A. Lindgård and O. G. Mouritsen, Phys. Rev. Lett. **57**, 2458 (1986).
[3] U. Pinsook and G. J. Ackland, Phys. Rev. B **58**, 11 252 (1998).
[4] R. Ahuja, J. M. Wills, B. Johansson, and O. Eriksson, Phys. Rev. B **48**, 16 269 (1993).
[5] C. Zener, Phys. Rev. **71**, 846 (1947).
[6] J. Friedel, J. Phys. (Paris) **35**, L59 (1974).
[7] C. Stassis, J. Zarestky, and N. Wakabayashi, Phys. Rev. Lett. **41**, 1726 (1978).
[8] C. Stassis and J. Zarestky, Solid State Commun. **52**, 9 (1984).
[9] A. Heiming, W. Petry, J. Trampenau, M. Alba, C. Herzig, H. R. Schöber, and G. Vogl, Phys. Rev. B **43**, 10 948 (1991).
[10] O. Dubos, W. Petry, J. Neuhaus, and B. Hennion, Eur. Phys. J. B **3**, 447 (1998).
[11] T. May, W. Müller, and D. Strauch, Phys. Rev. B **57**, 5758 (1998).
[12] Y.-Y. Ye, Y. Chen, K.-M. Ho, B. N. Harmon, and P.-A. Lindgård, Phys. Rev. Lett. **58**, 1769 (1987).
[13] F. Willaime and C. Massobrio, Phys. Rev. Lett. **63**, 2244 (1989).
[14] F. Willaime and C. Massobrio, Phys. Rev. B **43**, 11 653 (1991).
[15] W. C. Kerr and M. J. Rave, Phys. Rev. B **48**, 16 234 (1993).
[16] J. R. Morris and R. J. Gooding, Phys. Rev. B **43**, 6057 (1991).
[17] J. R. Morris and R. J. Gooding, Phys. Rev. B **46**, 8733 (1992).
[18] S. Rubini and P. Ballone, Phys. Rev. B **48**, 99 (1993).
[19] P.-A. Lindgård and O. G. Mouritsen, Phys. Rev. B **41**, 688 (1990).
[20] R. J. Gooding and J. A. Krumhansl, Phys. Rev. B **38**, 1695 (1988).
[21] P. J. Craievich, J. M. Sanchez, R. E. Watson, and M. Weinert, Phys. Rev. B **55**, 787 (1997).
[22] E. G. Moroni, G. Grimvall, and T. Jarlborg, Phys. Rev. Lett. **76**, 2758 (1996).
[23] J. Gavartin (private communication).
[24] M. W. Finnis and J. F. Sinclair, Philos. Mag. A **50**, 45 (1984); **53**, 161 (1986).
[25] G. J. Ackland, M. W. Finnis, and V. Vitek, J. Phys. F **18**, L153 (1988).
[26] G. J. Ackland, G. I. Tichy, V. Vitek, and M. W. Finnis, Philos. Mag. A **56**, 735 (1987).
[27] G. J. Ackland, S. J. Wooding, and D. J. Bacon, Philos. Mag. A **71**, 553 (1995).
[28] G. J. Ackland, Ph.D. thesis, Oxford University, 1987.
[29] M. W. Finnis, UKAEA Report No. AERE R13182, 1988 (unpublished).
[30] S. Nosé, Mol. Phys. **50**, 255 (1984).
[31] S. Nosé, J. Chem. Phys. **81**, 511 (1984).
[32] W. G. Hoover, Phys. Rev. A **31**, 1695 (1985).
[33] J. M. Dickey and A. Paskin, Phys. Rev. **188**, 1407 (1969).
[34] M. Born and K. Huang, *Dynamical Theory of Crystal Lattices* (Oxford University Press, London, 1956).
[35] G. J. Ackland, in *Alloy Modeling and Design* (TMS93 proceedings), edited by G. M. Stocks and P. E. A. Turchi (TMS, The Minerals, Metals and Materials Society, Warrendale, PA, 1993), p. 149.
[36] There are 12 symmetrically equivalent N points in the bcc Brillouin zone, but because of inversion symmetry these give rise to only six inequivalent martensitic variants.
[37] At 1400 K the bcc structure remains stable for only a few picoseconds before returning to hcp. The reason for this is unclear: it is possible that the strain on the unit cell is unable to relax quickly enough to fully stabilize the bcc. The microstructure of the recovered hcp is the same as the starting martensite configuration, indicating that the structure has retained some memory of its previous structure.
[38] Y. N. Osetsky and A. Serra, Phys. Rev. B **57**, 755 (1998).